Search for time-independent Lorentz violation using muon neutrino to muon antineutrino transitions in MINOS

P. Adamson,[8] I. Anghel,[15,1] A. Aurisano,[7] G. Barr,[22] M. Bishai,[3] A. Blake,[5,16] G. J. Bock,[8] D. Bogert,[8] S. V. Cao,[30] T. J. Carroll,[30] C. M. Castromonte,[9] R. Chen,[18] S. Childress,[8] J. A. B. Coelho,[31] L. Corwin,[14,*] D. Cronin-Hennessy,[19] J. K. de Jong,[22] S. de Rijck,[30] A. V. Devan,[33] N. E. Devenish,[28] M. V. Diwan,[3] C. O. Escobar,[6] J. J. Evans,[18] E. Falk,[28] G. J. Feldman,[10] W. Flanagan,[30] M. V. Frohne,[11,†] M. Gabrielyan,[19] H. R. Gallagher,[31] S. Germani,[17] R. A. Gomes,[9] M. C. Goodman,[1] P. Gouffon,[25] N. Graf,[13,23] R. Gran,[20] K. Grzelak,[32] A. Habig,[20] S. R. Hahn,[8] J. Hartnell,[28] R. Hatcher,[8] A. Holin,[17] J. Huang,[30] J. Hylen,[8] G. M. Irwin,[27] Z. Isvan,[3,23] C. James,[8] D. Jensen,[8] T. Kafka,[31] S. M. S. Kasahara,[19] G. Koizumi,[8] M. Kordosky,[33] A. Kreymer,[8] K. Lang,[30] J. Ling,[3] P. J. Litchfield,[19,24] P. Lucas,[8] W. A. Mann,[31] M. L. Marshak,[19] N. Mayer,[31,14] C. McGivern,[23] M. M. Medeiros,[9] R. Mehdiyev,[30] J. R. Meier,[19] M. D. Messier,[14] W. H. Miller,[19] S. R. Mishra,[26] S. Moed Sher,[8] C. D. Moore,[8] L. Mualem,[4] J. Musser,[14] D. Naples,[23] J. K. Nelson,[33] H. B. Newman,[4] R. J. Nichol,[17] J. A. Nowak,[19,‡] J. O'Connor,[17] M. Orchanian,[4] R. B. Pahlka,[8] J. Paley,[1] R. B. Patterson,[4] G. Pawloski,[19,27] A. Perch,[17] M. M. Pfützner,[17] D. D. Phan,[30] S. Phan-Budd,[1] R. K. Plunkett,[8] N. Poonthottathil,[8] X. Qiu,[27] A. Radovic,[33] B. Rebel,[8] C. Rosenfeld,[26] H. A. Rubin,[13] P. Sail,[30] M. C. Sanchez,[15,1] J. Schneps,[31] A. Schreckenberger,[30,19] P. Schreiner,[1] R. Sharma,[8] A. Sousa,[7,10] N. Tagg,[21] R. L. Talaga,[1] J. Thomas,[17] M. A. Thomson,[5] X. Tian,[26] A. Timmons,[18] J. Todd,[7] S. C. Tognini,[9] R. Toner,[10,5] D. Torretta,[8] G. Tzanakos,[2,†] J. Urheim,[14] P. Vahle,[33] B. Viren,[3] A. Weber,[22,24] R. C. Webb,[29] C. White,[13] L. Whitehead,[12,3] L. H. Whitehead,[17] S. G. Wojcicki,[27] and R. Zwaska[8]

(The MINOS Collaboration)

[1] *Argonne National Laboratory, Argonne, Illinois 60439, USA*
[2] *Department of Physics, University of Athens, GR-15771 Athens, Greece*
[3] *Brookhaven National Laboratory, Upton, New York 11973, USA*
[4] *Lauritsen Laboratory, California Institute of Technology, Pasadena, California 91125, USA*
[5] *Cavendish Laboratory, University of Cambridge, Cambridge CB3 0HE, United Kingdom*
[6] *Universidade Estadual de Campinas, IFGW, CP 6165, 13083-970, Campinas, SP, Brazil*
[7] *Department of Physics, University of Cincinnati, Cincinnati, Ohio 45221, USA*
[8] *Fermi National Accelerator Laboratory, Batavia, Illinois 60510, USA*
[9] *Instituto de Física, Universidade Federal de Goiás, 74690-900, Goiânia, GO, Brazil*
[10] *Department of Physics, Harvard University, Cambridge, Massachusetts 02138, USA*
[11] *Holy Cross College, Notre Dame, Indiana 46556, USA*
[12] *Department of Physics, University of Houston, Houston, Texas 77204, USA*
[13] *Department of Physics, Illinois Institute of Technology, Chicago, Illinois 60616, USA*
[14] *Indiana University, Bloomington, Indiana 47405, USA*
[15] *Department of Physics and Astronomy, Iowa State University, Ames, Iowa 50011 USA*
[16] *Lancaster University, Lancaster, LA1 4YB, UK*
[17] *Department of Physics and Astronomy, University College London, London WC1E 6BT, United Kingdom*
[18] *School of Physics and Astronomy, University of Manchester, Manchester M13 9PL, United Kingdom*
[19] *University of Minnesota, Minneapolis, Minnesota 55455, USA*
[20] *Department of Physics, University of Minnesota Duluth, Duluth, Minnesota 55812, USA*
[21] *Otterbein University, Westerville, Ohio 43081, USA*
[22] *Subdepartment of Particle Physics, University of Oxford, Oxford OX1 3RH, United Kingdom*
[23] *Department of Physics and Astronomy, University of Pittsburgh, Pittsburgh, Pennsylvania 15260, USA*
[24] *Rutherford Appleton Laboratory, Science and Technology Facilities Council, Didcot, OX11 0QX, United Kingdom*
[25] *Instituto de Física, Universidade de São Paulo, CP 66318, 05315-970, São Paulo, SP, Brazil*
[26] *Department of Physics and Astronomy, University of South Carolina, Columbia, South Carolina 29208, USA*
[27] *Department of Physics, Stanford University, Stanford, California 94305, USA*
[28] *Department of Physics and Astronomy, University of Sussex, Falmer, Brighton BN1 9QH, United Kingdom*
[29] *Physics Department, Texas A&M University, College Station, Texas 77843, USA*
[30] *Department of Physics, University of Texas at Austin, Austin, Texas 78712, USA*
[31] *Physics Department, Tufts University, Medford, Massachusetts 02155, USA*
[32] *Department of Physics, University of Warsaw, PL-02-093 Warsaw, Poland*
[33] *Department of Physics, College of William & Mary, Williamsburg, Virginia 23187, USA*

(Dated: January 15, 2019)

Data from the MINOS experiment has been used to search for mixing between muon neutrinos and muon antineutrinos using a time-independent Lorentz-violating formalism derived from

the Standard-Model Extension (SME). MINOS is uniquely capable of searching for muon neutrino-antineutrino mixing given its long baseline and ability to distinguish between neutrinos and antineutrinos on an event-by-event basis. Neutrino and antineutrino interactions were observed in the MINOS Near and Far Detectors from an exposure of 10.56×10^{20} protons-on-target from the NuMI neutrino-optimized beam. No evidence was found for such transitions and new, highly stringent limits were placed on the SME coefficients governing them. We place the first limits on the SME parameters $(c_L)^{TT}_{\mu\mu}$ and $(c_L)^{TT}_{\tau\tau}$ at $-8.4\times10^{-23} < (c_L)^{TT}_{\mu\mu} < 8.0\times10^{-23}$ and $-8.0\times10^{-23} < (c_L)^{TT}_{\tau\tau} < 8.4\times10^{-23}$, and the world's best limits on the $\tilde{g}^{ZT}_{\mu\overline{\mu}}$ and $\tilde{g}^{ZT}_{\tau\overline{\tau}}$ parameters at $|\tilde{g}^{ZT}_{\mu\overline{\mu}}| < 3.3\times10^{-23}$ and $|\tilde{g}^{ZT}_{\tau\overline{\tau}}| < 3.3\times10^{-23}$, all limits quoted at 3σ.

PACS numbers: 11.30Cp, 14.60.Pq, 14.60.St

The modified Standard Model (SM) of particle physics formed by adding neutrino masses to the SM, also called the neutrino Standard Model (νSM), has been successful in explaining most of the neutrino oscillation experimental results to date [1]. The Standard-Model Extension (SME) [2–4] is an effective field theory that provides a framework for inclusion of coordinate-independent Lorentz violation and CPT violation into the νSM. The operators for Lorentz and CPT violation are controlled by a set of coefficients whose values are to be determined or constrained by experiment. CPT and Lorentz symmetries are fundamental to the νSM and any evidence of their violation would necessitate fundamental changes in the theories of gravity and quantum mechanics. Searching for Lorentz and CPT violation in the neutrino sector was originally proposed in 1997 [2]. Several testable models have since been developed using a subset of the SME neutrino-sector coefficients [5]. Constraints on a number of SME coefficients have been obtained by various experiments including MINOS [6–11]. The analysis presented in this paper places the strongest constraints on the time-independent SME coefficients in the μ-τ sector.

Long-baseline neutrino oscillation experiments are sensitive to Lorentz and CPT violation. These effects can be tested through searches for oscillations that deviate from the standard L/E dependence (this analysis), where L is the neutrino propagation distance and E is the neutrino energy, or through searches for sidereal time-dependent variations in event rate as a consequence of a preferred direction in the universe [6–10]. A two-flavor model can be constructed that assumes the Lorentz-violating flavor change occurs in the muon to tau flavor transition. This model, adapted from [12], simplifies the SME formalism, allowing limits to be set on a subset of four of its components [13]. The frame of reference for the present study is the Sun-centered celestial coordinate system with coordinates (T, X, Y, Z). In this frame the spatial origin is fixed at the Sun's center with the Z axis pointing north and parallel to the Earth's rotation axis. The X and Y axes are in the equatorial plane, the X axis pointing towards the vernal equinox and the Y axis completing the right-handed coordinate system. The time T is measured by a clock at rest at the origin, with T=0 taken as the vernal equinox in the year 2000. The SME coefficients controlling Lorentz violation are $\tilde{g}^{ZT}_{\mu\overline{\mu}}$, $\tilde{g}^{ZT}_{\tau\overline{\tau}}$, $(c_L)^{TT}_{\mu\mu}$, and $(c_L)^{TT}_{\tau\tau}$. The lepton number violating neutrino-antineutrino mixing is controlled by the coefficients $\tilde{g}^{AB}_{\mu\overline{\mu}}$ and $\tilde{g}^{AB}_{\tau\overline{\tau}}$, where the space-time indices A and B are either Z or T. The contribution to neutrino-neutrino mixing is controlled by the coefficients $(c_L)^{TT}_{\mu\mu}$ and $(c_L)^{TT}_{\tau\tau}$.

The oscillation probabilities in this model, expressed in natural units, are:

Survival probability of ν_μ:

$$P(\nu_\mu \to \nu_\mu) = 1 - \Big(\sin^2(\theta_{C\text{-}odd} - \theta_{C\text{-}even}) + \frac{1}{4}\left[\sin(2\theta_{C\text{-}odd}) + \sin(2\theta_{C\text{-}even})\right]^2\Big)\sin^2\left(\frac{\Delta m^2 L}{4E}\right). \quad (1)$$

Oscillation probability ν_μ to $\overline{\nu}_\mu$:

$$P(\nu_\mu \to \overline{\nu}_\mu) = \Big(\sin^2(\theta_{C\text{-}odd} - \theta_{C\text{-}even}) - \frac{1}{4}\left[\sin(2\theta_{C\text{-}odd}) - \sin(2\theta_{C\text{-}even})\right]^2\Big)\sin^2\left(\frac{\Delta m^2 L}{4E}\right). \quad (2)$$

Oscillation probability ν_μ to ν_τ:

$$P(\nu_\mu \to \nu_\tau) = \Big(\frac{1}{4}\left[\sin(2\theta_{C\text{-}odd}) + \sin(2\theta_{C\text{-}even})\right]^2\Big)\sin^2\left(\frac{\Delta m^2 L}{4E}\right). \quad (3)$$

Oscillation probability of ν_μ to $\overline{\nu}_\tau$:

$$P(\nu_\mu \to \overline{\nu}_\tau) = \Big(\frac{1}{4}\left[\sin(2\theta_{C\text{-}odd}) - \sin(2\theta_{C\text{-}even})\right]^2\Big)\sin^2\left(\frac{\Delta m^2 L}{4E}\right). \quad (4)$$

Here Δm^2 is the mass-squared difference between neutrino mass eigenstates, assumed to be identical to the mass-squared difference between antineutrino mass eigenstates; L is the neutrino propagation length and E is the neutrino energy; and $\theta_{C\text{-}odd}$ and $\theta_{C\text{-}even}$ are the effective mixing angles for states that are odd and even, respectively, under the charge conjugation operator C in flavor space [12]. The angles $\theta_{C\text{-}odd}$ and $\theta_{C\text{-}even}$ are related to the mixing angle θ describing oscillations in a two-flavor model:

$$\theta_{C\text{-}odd} = \frac{1}{2}\tan^{-1}\left(\frac{\Delta m^2 \sin 2\theta}{[1.6(\tilde{g}^{ZT}_{\mu\overline{\mu}} - \tilde{g}^{ZT}_{\tau\overline{\tau}}) + 2.7((c_L)^{TT}_{\mu\mu} - (c_L)^{TT}_{\tau\tau})]E^2 + \Delta m^2 \cos 2\theta}\right), \quad (5)$$

$$\theta_{C\text{-}even} = \frac{1}{2}\tan^{-1}\left(\frac{\Delta m^2 \sin 2\theta}{[-1.6(\tilde{g}^{ZT}_{\mu\overline{\mu}} - \tilde{g}^{ZT}_{\tau\overline{\tau}}) + 2.7((c_L)^{TT}_{\mu\mu} - (c_L)^{TT}_{\tau\tau})]E^2 + \Delta m^2 \cos 2\theta}\right). \quad (6)$$

Here, both E^2 and Δm^2 are expressed in units of eV^2. The factors of 1.6 and 2.7 appearing in equations (5) and (6) are derived from the colatitude, zenith, and azimuthal angles of the beam following Ref. [12, 13]; the values of those angles for this study are given in the experimental description below. The effect of the $\tilde{g}^{ZT}_{\mu\overline{\mu}}$ coefficients on the neutrino-antineutrino oscillations is shown, as a function of neutrino energy, in Fig. 1. The effect of the $\tilde{g}^{ZT}_{\tau\overline{\tau}}$ parameters is the same, but with the dashed and solid lines swapped. At low energies, there are no neutrino-antineutrino transitions. At high energies, the effective mixing between neutrino and antineutrino states becomes maximal. In the case that the c-type coefficients are zero, the threshold for significant neutrino-antineutrino mixing to occur can be calculated by making the denominator of equations (5) and (6) approach zero. This threshold happens in the region of $E = \sqrt{\Delta m^2/1.6(\tilde{g}^{ZT}_{\alpha\overline{\alpha}})}$ eV, where α can be either μ or τ. As can be seen from equations (5) and (6), if the g-type coefficients are set to zero, then $\theta_{C\text{-}odd}$ and $\theta_{C\text{-}even}$ are equal. Hence, c-type coefficients alone cannot cause neutrino-antineutrino transitions.

The coefficients constrained in this analysis are different from the neutrino-antineutrino mixing coefficients constrained in the previous MINOS analyses where the space-time indices AB were $XT, YT, XZ, YZ, ZX, ZY, XX, YY, XY, YX$ and flavor indices were $e\overline{e}, e\overline{\mu}, e\overline{\tau}, \mu\overline{\mu}, \mu\overline{\tau}, \tau\overline{\tau}$, which would lead to sidereal variations in the normalized event rate. The coefficients having space-time indices TT and ZT do not give rise to sidereal variations.

MINOS is a long-baseline experiment that measures the oscillations of muon neutrinos and antineutrinos in the NuMI beam [14] using two detectors. These detectors are steel-scintillator tracking calorimeters with a toroidal magnetic field of approximately 1.4 T [15]. The 0.98 kton Near Detector (ND) is located at Fermilab and is used to measure the neutrino and antineutrino energy spectra 1.04 km downstream of the production target. The 5.4 kton Far Detector (FD) is located in the Soudan Mine in Minnesota and is used to measure the energy spectra 735 km from the target. The NuMI beam is produced at Fermilab by 120 GeV protons striking a graphite target. The colatitude of the NuMI beam is $\chi = 42.17973347°$, the beam zenith angle is $\theta = 86.7255°$, measured from the z-axis, and the beam azimuthal angle is $\phi = 203.909°$,

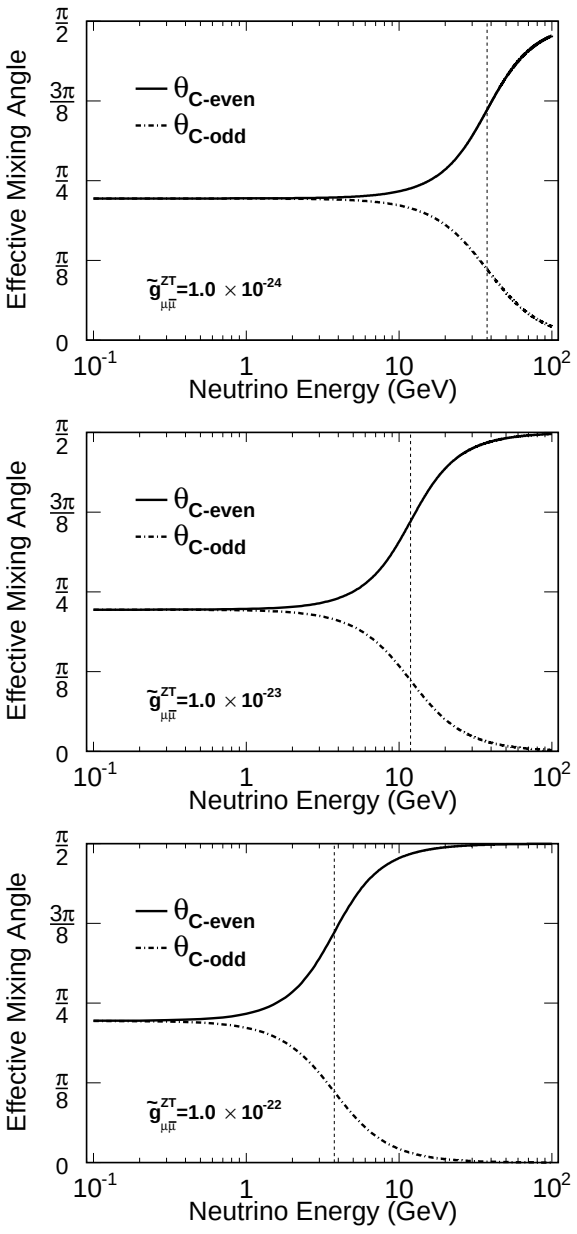

FIG. 1: The graphs show the effective mixing angles $\theta_{C\text{-}odd}$ or $\theta_{C\text{-}even}$ as a function of neutrino energy E for three different values of $\tilde{g}^{ZT}_{\mu\overline{\mu}}$. We have chosen $\Delta m^2 = 2.32\times10^{-3}\mathrm{eV}^2$, $\sin^2 2\theta = 0.97$, and $\tilde{g}^{ZT}_{\tau\overline{\tau}} = (c_L)^{TT}_{\mu\mu} = (c_L)^{TT}_{\tau\tau} = 0$. The values of Δm^2 and $\sin^2 2\theta$ are taken from [17]. The dotted vertical line is drawn at $E = \sqrt{\Delta m^2/1.6(\tilde{g}^{ZT}_{\mu\overline{\mu}})}$ eV.

measured counterclockwise from the x-axis, which points south. The composition of the neutrino-optimized beam, as measured in the ND, is 91.7% ν_μ, 7% $\overline{\nu}_\mu$, and 1.3% ν_e+ $\overline{\nu}_e$. The results presented here are based on the analysis of muon neutrinos and antineutrinos selected in an exposure of 10.56×10^{20} protons-on-target of the beam obtained between May, 2005 and April, 2012. This data was acquired in the "low energy" NuMI beam configuration [14], where the neutrino event energy peaks at 3 GeV.

The muon neutrinos and antineutrinos are identified by their charged-current (CC) interactions

$$\nu_\mu(\overline{\nu}_\mu) + X \rightarrow \mu^-(\mu^+) + X', \tag{7}$$

where a muon track and a hadronic shower (X') may be observed. The selection of CC interactions is described in detail in previous publications [16–18]. The standard MINOS procedure is to calculate the total reconstructed neutrino energy of the interaction by summing the energies of the reconstructed μ^- or μ^+ track and the hadronic shower. Selected ν_μ and $\overline{\nu}_\mu$ CC events contain at least one reconstructed track and originate inside the fiducial volume of the detectors. The hadronic energy is determined using calorimetry by summing the pulse height of all hits clustered in the shower region. For muons that stop inside the detector, the muon energy is measured using the length of the muon track. If the muon exits the detector, the curvature of the muon in the magnetic field is used to determine its energy. For this dataset, the magnetic fields in both detectors are such that they focus μ^- and defocus μ^+.

In the ν_μ sample the largest background arises from the neutral-current (NC) interactions in which a track is reconstructed and misidentified as a muon track. The dominant backgrounds in the $\overline{\nu}_\mu$ sample are ν_μ events selected as $\overline{\nu}_\mu$ due to misidentification of muon charge, and NC interactions. An optimized $\overline{\nu}_\mu$ event selection is applied to increase the purity of this sample [18, 19]. The $\overline{\nu}_\mu$ events are selected using three variables. Two of the variables are used to correctly identify the charge sign of the muon track, and the third is a likelihood-based CC/NC separation parameter. The separation parameter is constructed from 1-dimensional probability density functions of three variables describing track properties. FD selection efficiencies for neutrino and antineutrino samples are 90% and 89%, respectively, and purities are approximately 98% for both.

The ND data is used to make a prediction of neutrino and antineutrino spectra at the FD by using a beam transfer matrix which takes into account the differences in the geometric acceptance of the two detectors [20, 21]. This FD prediction is then compared to the data from the FD. This comparison allows for cancellation of a number of systematic uncertainties that affect both the detectors in the same way.

In this work we present new results on the limits on the SME parameters $\tilde{g}^{ZT}_{\mu\overline{\mu}}$, $\tilde{g}^{ZT}_{\tau\overline{\tau}}$, $(c_L)^{TT}_{\mu\mu}$, and $(c_L)^{TT}_{\tau\tau}$. MINOS has previously reported two-flavor oscillation analysis results using the neutrino [17] as well as the antineutrino [18] samples in this dataset. Limits are placed on the $\tilde{g}$ parameters through our sensitivity to the oscillation of muon neutrino events into muon antineutrino events. Such oscillations would be seen as an excess of the antineutrino events at the FD as compared to the number predicted from standard oscillations by independently varying each parameter by its systematic uncertainties.

Several sources of systematic uncertainty can affect this search for an excess of $\overline{\nu}_\mu$ events at the FD. For each source of uncertainty, Monte Carlo spectra were generated by varying each parameter by the $\pm 1\sigma$ value of the systematic uncertainty independently. The shifted neutrino and antineutrino sets were fit simultaneously to the parameters $\tilde{g}^{ZT}_{\alpha\overline{\alpha}}$ and $(c_L)^{TT}_{\alpha\alpha}$ using a binned log-likelihood method. The shifts in the best-fit values of $\tilde{g}^{ZT}_{\alpha\overline{\alpha}}$ and $(c_L)^{TT}_{\alpha\alpha}$ are shown in Table I, along with the shift in the value of χ^2 at the best-fit point. The systematics with the largest change in the value of χ^2 were found to be the hadronic energy scale, muon energy scale, and the relative normalization between the Near and Far Detectors. The relative normalization uncertainty is 1.6% for muon neutrino events [17] and 4% for muon antineutrino events [18]. This uncertainty is a combination of the uncertainties in the difference in reconstruction efficiencies, the difference in live times, and the structural differences between the Near and Far Detectors. The uncertainty on the measurement of muon momentum measured using its range is 2% for both neutrinos and antineutrinos, and that on the muon momentum from curvature is 3% for neutrinos and 4% for antineutrinos. The positive muons created due to the interaction of antineutrinos in the detector are defocused by the magnetic fields in the detectors and have shorter lengths. Hence antineutrinos have a larger uncertainty on the momentum measurement as compared to neutrinos. The uncertainty in the hadronic energy measurement consists of two components. One component is fully correlated between both detectors, and comes from calibration and shower modeling uncertainties. It can be parametrized as $(6.6 + 3.5\mathrm{e}^{-E_{shw}/1.44\mathrm{GeV}})\%$ [22]. The second component, dominated by calibration uncertainties, is uncorrelated between the detectors. This component has a magnitude of 1.9% for the ND and 1.1% for the FD.

We now describe the procedure to calculate the sensitivity to the SME coefficients. Beginning with all SME coefficients set to zero, and allowing a single coefficient to vary at a time, a 3σ sensitivity can be achieved for $|\tilde{g}^{ZT}_{\alpha\overline{\alpha}}|$ at 3.4×10^{-23} and $(c_L)^{TT}_{\alpha\alpha}$ at 6×10^{-23}. The FD antineutrino and neutrino spectra expected when $\tilde{g}^{ZT}_{\alpha\overline{\alpha}} = 3.4 \times 10^{-23}$ are shown in Fig. 2. The energy at which the excess in the antineutrino spectrum is expected decreases when the values of these parameters are increased due to lowering of the energy threshold at which significant neutrino-antineutrino transitions can occur. The expected FD antineutrino and neutrino spec-

tra for $(c_L)^{TT}_{\mu\mu} = 6\times10^{-23}$ are also shown in Fig. 2. These coefficients only change the mixing between the neutrinos and not that of antineutrinos with neutrinos.

Uncertainty	$\Delta\tilde{g}$	Δc	$\Delta(\chi^2)$
Hadronic energy	1.8×10^{-27}	6.4×10^{-24}	2.67
Muon energy	5.1×10^{-27}	4.6×10^{-24}	2.04
Relative normalization	5.9×10^{-24}	7.3×10^{-24}	0.60
All other uncertainties	3.3×10^{-24}	6.5×10^{-24}	0.14
Statistical Error	1.6×10^{-23}	1.6×10^{-23}	1.00

TABLE I: Shifts in the measurements of the parameters $\tilde{g}^{ZT}_{\alpha\overline{\alpha}}$ and $(c_L)^{TT}_{\alpha\alpha}$ between the unshifted and shifted best-fit points for each source of systematic uncertainty. Also shown is the change in the value of χ^2 at best-fit. (Input: $\Delta m^2 = 2.32\times10^{-3}\text{eV}^2, \sin^2 2\theta = 0.97, \tilde{g} \equiv \tilde{g}^{ZT}_{\alpha\overline{\alpha}} = 0, c \equiv (c_L)^{TT}_{\alpha\alpha} = 0$). The last row shows the size of the statistical error.

The fit to the data is performed by minimizing a log-likelihood function. Neutrinos with reconstructed energies below 50 GeV are used in the fit. Scans of either $\tilde{g}^{ZT}_{\alpha\overline{\alpha}}$ or $(c_L)^{TT}_{\alpha\alpha}$ parameters are performed with the other parameter set to zero, and Δm^2 and $\sin^2 2\theta$ are marginalized for each value of the parameter. The three largest sources of systematic uncertainty, as shown in Table I, are included in the fit as nuisance parameters. The function to be minimized can be written as:

$$-2\log\lambda = 2\sum_{i=1}^{n}\left[P_i - D_i + D_i\ln\left(\frac{D_i}{P_i}\right)\right] + \sum_{j=1}^{3}\frac{\epsilon_j^2}{\sigma_j^2}, \quad (8)$$

where P_i is the expected number of events based on the FD prediction and D_i is the number of events from FD data in bin i. The nuisance parameter ϵ_j corresponds to the shift from the nominal value of the j^{th} source of systematic uncertainty and σ_j is the uncertainty of the j^{th} source. The value of the mixing angle is kept physical by constraining $0 \le \sin^2 2\theta \le 1$. As shown in the last row of Table I the effect of systematic uncertainties on the measurement of the parameters $\tilde{g}^{ZT}_{\alpha\overline{\alpha}}$ and $(c_L)^{TT}_{\alpha\alpha}$ is smaller than the statistical uncertainty.

Fig. 3 shows the log-likelihood values, obtained from the data, for $|\tilde{g}^{ZT}_{\alpha\overline{\alpha}}|$ and $(c_L)^{TT}_{\alpha\alpha}$, with the 1σ, 2σ, and 3σ limits indicated by the dotted lines. Only the positive part of the x-axis is shown for the limit on the g parameters because the positive and negative halves are perfectly symmetrical, as seen from Equations (5) and (6). From the same equations it is seen that the limits on $(c_L)^{TT}_{\mu\mu}$ will be the same as the limits on -$(c_L)^{TT}_{\tau\tau}$. The 3σ upper limits obtained for these parameters are tabulated in Table II. The values for Δm^2 and $\sin^2 2\theta$ at the best-fit point are consistent with those in [17]. The resulting FD simulated energy spectra, obtained by using the best-fit values, are shown in Fig. 4 along with the neutrino and antineutrino spectra. Also shown are the FD spectra expected using the 2-flavor oscillation model.

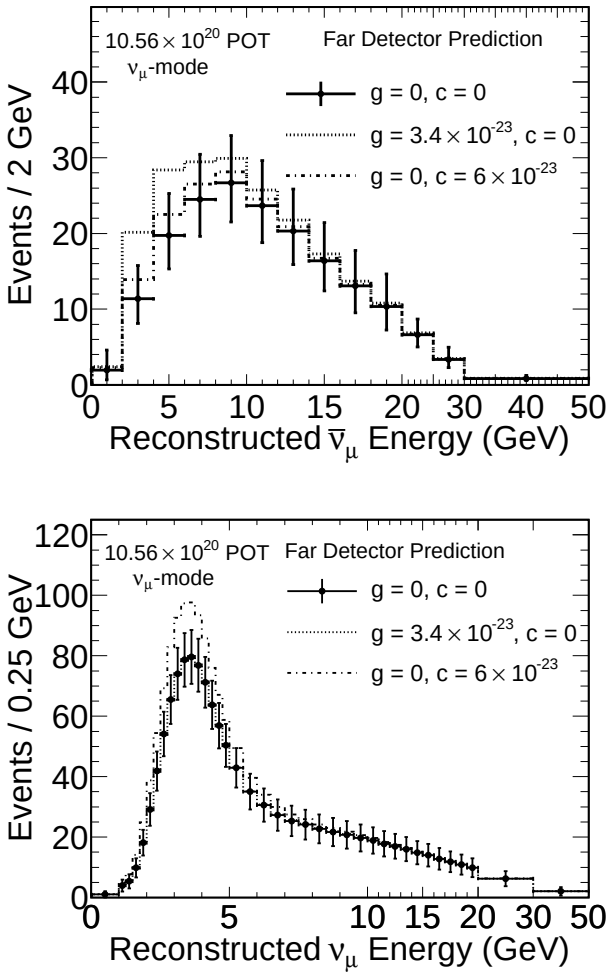

FIG. 2: FD neutrino spectra expected at different values of $\tilde{g}^{ZT}_{\alpha\overline{\alpha}}$ and $(c_L)^{TT}_{\alpha\alpha}$. The bold dots, shown with statistical errors, show the spectrum when both the SME coefficients are zero. The dotted histogram shows the FD spectrum predicted at $\tilde{g}^{ZT}_{\alpha\overline{\alpha}} = 3.4\times10^{-23}$ and the dotted-dashed histogram shows the FD prediction at $(c_L)^{TT}_{\alpha\alpha} = 6\times10^{-23}$. The values of parameters chosen correspond to the 3σ sensitivity limit. Most of the power in fitting for $\tilde{g}^{ZT}_{\alpha\overline{\alpha}}$ comes from the antineutrino spectrum and that for $(c_L)^{TT}_{\alpha\alpha}$ comes from the neutrino spectrum.

The spectra obtained using the best-fit parameters from the SME model are seen to be almost indistinguishable from the 2-flavor prediction.

Limit set by this work	Previous best limit
$\lvert\tilde{g}^{ZT}_{\mu\overline{\mu}}\rvert < 3.3\times10^{-23}$	2.3×10^{-16} [11]
$\lvert\tilde{g}^{ZT}_{\tau\overline{\tau}}\rvert < 3.3\times10^{-23}$	2.3×10^{-16} [11]
$-8.4\times10^{-23} < (c_L)^{TT}_{\mu\mu} < 8.0\times10^{-23}$	–
$-8.0\times10^{-23} < (c_L)^{TT}_{\tau\tau} < 8.4\times10^{-23}$	–

TABLE II: 3σ upper and lower limits on the SME coefficients describing time-independent Lorentz violation.

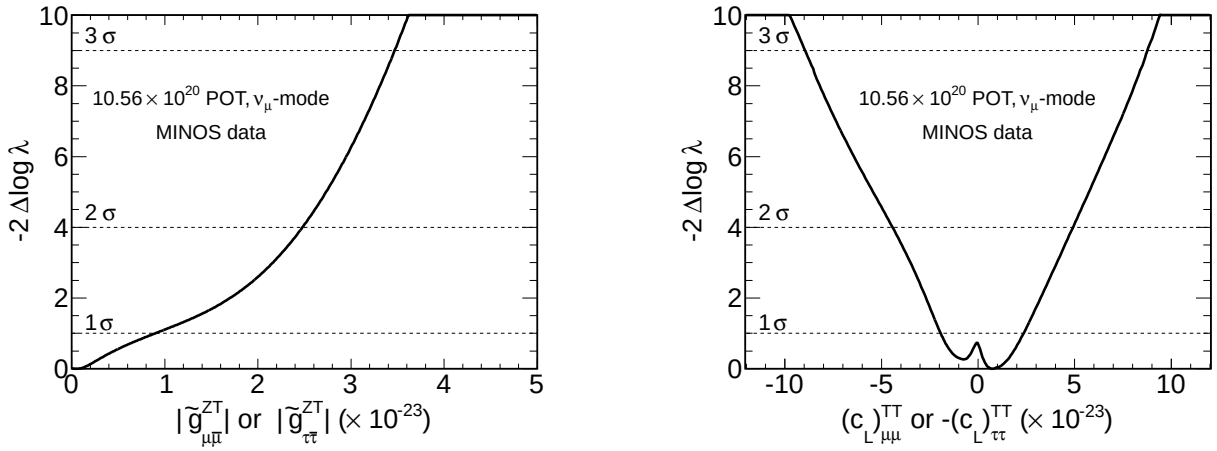

FIG. 3: The log-likelihood values for the $|\tilde{g}^{ZT}_{\alpha\overline{\alpha}}|$ and $(c_L)^{TT}_{\mu\mu}$ parameters, with the 1σ, 2σ, and 3σ limits indicated by the dotted lines. Limits on $(c_L)^{TT}_{\mu\mu}$ are by construction the limits on -$(c_L)^{TT}_{\tau\tau}$.

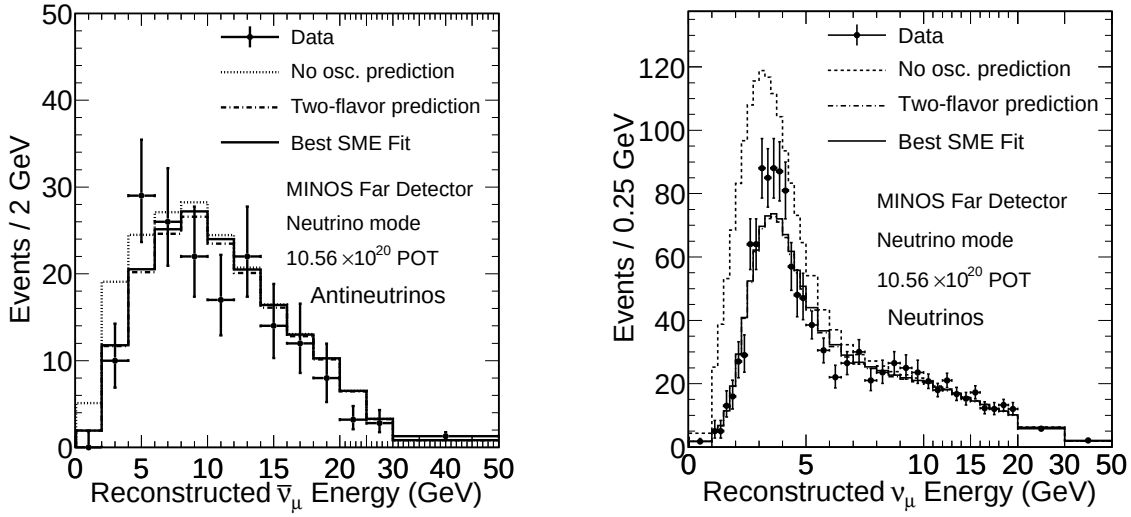

FIG. 4: Far Detector distributions of selected antineutrino (left) and neutrino (right) events. Black dots represent data, the dashed histogram shows the prediction in the absence of oscillations, the dotted-dashed histogram shows the prediction at the values obtained in a fit to 2-flavor oscillation model, and the solid histogram shows the prediction at the values obtained in our fit to the SME model. The prediction obtained in a fit to a two-flavor oscillation model is very similar to that obtained from the SME fit.

In summary, the MINOS data collected in the neutrino-optimized mode has been used to search for evidence of Lorentz and CPT violation and no indication for the violation of these symmetries has been found. This data has been used to set the world's leading experimental constraints on the SME coefficients: $\tilde{g}^{ZT}_{\mu\overline{\mu}}$, $\tilde{g}^{ZT}_{\tau\overline{\tau}}$, $(c_L)^{TT}_{\mu\mu}$, and $(c_L)^{TT}_{\tau\tau}$.

This work was supported by the US DOE, the UK STFC, the US NSF, the State and University of Minnesota, the University of Athens, Greece, and Brazil's FAPESP, CNPq and CAPES. We are grateful to the Minnesota Department of Natural Resources, the crew of the Soudan Underground Laboratory, and the staff of Fermilab for their contributions to this effort.

* Now at South Dakota School of Mines and Technology, Rapid City, South Dakota 57701, USA.

† Deceased.

‡ Now at Lancaster University, Lancaster, LA1 4YB, UK.

[1] K. A. Olive *et al.* (Particle Data Group), Chin. Phys. C **38**, 090001 (2014), Chapter 14, "Neutrino mass, mixing, and oscillations," by K. Nakamura and S. T. Petcov.

[2] D. Colladay and V. A. Kostelecký, Phys. Rev. D **55**, 6760 (1997).

[3] D. Colladay and V. A. Kostelecký, Phys. Rev. D **58**, 116002 (1998); V. A. Kostelecký, Phys. Rev. D **69**, 105009 (2004).

[4] R. Bluhm, Lec. Notes Phys. **702**, 191 (2006), hep-ph/0506054; V. A. Kostelecký and N. Russell, Rev. Mod. Phys. **83**, 11 (2011).

[5] S. Coleman and S. L. Glashow, Phys. Rev. D **59**, 116008 (1999); V. Barger *et al.* Phys. Rev. Lett. **85**, 5055 (2000); J. N. Bahcall, V. Barger, and D. Marfatia, Phys. Lett. B **534**, 120 (2002); A. de Gouvêa, Phys. Rev. D **66**, 076005 (2002); G. Lambiase, Phys. Lett. B **560**, 1 (2003); A. Datta *et al.* Phys. Lett. B **597**, 356 (2004); S. Choubey and S. F. King, Phys. Lett. B **586**, 353 (2004); J. S. Diaz, V. A. Kostelecký, and M. Mewes, Phys. Rev. D. **80**, 076007 (2009).

[6] V. A. Kostelecký and N. Russell, Data Tables for Lorentz and CPT Violation, Rev. Mod. Phys. **83**, 11 (2011); T. Katori, Mod. Phys. Lett. A **27**, 1230024 (2012); A. A. Aguilar-Arevalo *et al.* (MiniBooNE), Phys. Lett. B **718**, 1303 (2013); L. B. Auerbach *et al.* (LSND), Phys. Rev. D **72**, 076004 (2005); Y. Abe *et al.* (Double Chooz), Phys. Rev. D **86**, 112009 (2012).

[7] P. Adamson *et al.* (MINOS), Phys. Rev. Lett. **101**, 151601 (2008).

[8] P. Adamson *et al.* (MINOS), Phys. Rev. Lett. **105**, 151601 (2010).

[9] P. Adamson *et al.* (MINOS), Phys. Rev. D **85**, 031101(R) (2012).

[10] B. Rebel and S. Mufson, Astropart. Phys. **48**, 78 (2013).

[11] J. S. Diaz *et al.*, Phys. Lett. B **727**, 412 (2013).

[12] S. Hollenberg, O. Micu, and H. Pas, Phys. Rev. D **80**, 053010 (2009).

[13] V. A. Kostelecký and M. Mewes, Phys. Rev. D. **69**, 016005 (2004).

[14] P. Adamson *et al.* (MINOS), Nucl. Instrum. Meth. A **806**, 279 (2016).

[15] D. G. Michael *et al.* (MINOS), Nucl. Instrum. Meth. A **596**, 190 (2008).

[16] R. Ospanov, Ph. D. thesis, University of Texas at Austin, FERMILAB-THESIS-2008-04 (2008).

[17] P. Adamson *et al.* (MINOS), Phys. Rev. Lett. **106**, 181801 (2011).

[18] P. Adamson *et al.* (MINOS), Phys. Rev. D. **84**, 071103(R) (2011).

[19] A. I. Himmel, Ph. D thesis, California Institute of Technology, FERMILAB-THESIS-2011-13 (2011).

[20] D. G. Michael *et al.* (MINOS), Phys. Rev. Lett. **97**, 191801 (2006); P. Adamson *et al.* (MINOS), Phys. Rev. D **77**, 072002 (2008).

[21] J. J. Evans, D. Phil. thesis, University of Oxford, FERMILAB-THESIS-2009-14 (2008).

[22] S. Dytman, H. Gallagher, and M. Kordosky, Proceedings of 10th International Workshop on Neutrino Factories, Super beams and Beta beams (Nufact08), June 30 - July 5 2008, Valencia, Spain PoS (NUFACT08).